

16. D. Cai et al., *J. Neurosci.* **21**, 4731 (2001).
17. M. U. Ehrengreuber et al., *Methods Enzymol.* **293**, 483 (1998).
18. J. L. Goldberg et al., *Neuron* **33**, 689 (2002).
19. A. Meyer-Franke et al., *Neuron* **21**, 681 (1998).
20. J. Du, L. Feng, F. Yang, B. Lu, *J. Cell Biol.* **150**, 1423 (2000).
21. S. Shen, A. P. Wiemelt, F. A. McMorris, B. A. Barres, *Neuron* **23**, 285 (1999).
22. F. L. Watson et al., *J. Neurosci.* **19**, 7889 (1999).
23. A signaling event is also consistent with the time course of change in axon growth rate (Fig. 1C): although RGCs are born in the retina over a period of 5 days between E13 and E18, we observed a sharp drop in 1 to 2 days in RGCs' intrinsic axon growth rate.
24. H. Mi, B. A. Barres, *J. Neurosci.* **19**, 1049 (1999).
25. C. L. Cepko, C. P. Austin, X. Yang, M. Alexiades, D. Ezzeddine, *Proc. Natl. Acad. Sci. U.S.A.* **93**, 589 (1996).
26. Serum drawn from rats on P0 or P1 was tested at final concentrations ranging from 0.1 to 10%. Retinoic acid and growth hormone were tested at 1 to 100 nM and 1 μ M, respectively. Conditioned medium from P8 tissues was also tested and showed no effect.
27. Further confirmation that this developmental switch was not attributable to target interaction was obtained by aspirating the superior colliculus from P0 animals, which did not prevent the decrease in intrinsic axon elongation ability.
28. Rat amacrine cells (9 to 12% of retinal neurons) were enriched to >85% purity by sequential immunopanning (13), depleting OX-7⁺ and RAN-2⁺ cells and then selecting VC1.1⁺ cells. Immunostaining with HPC-1, glial fibrillary acidic protein (GFAP), G26 (rhodopsin, courtesy of P. Hargrave), and Per3B6 (peripherin-2, courtesy of R. Molday) showed 85% amacrine, and <1% glia, rod, and cone photoreceptors. Amacrine 3-day survival was 75% on poly-D-lysine (PDL)-coated dishes in RGC growth media. Amacrine-depleted cultures consisted of all retinal cells not removed in the protocol above, largely photoreceptors and bipolar cells. Bipolar cells (4 to 6% of retinal neurons) were enriched from P12 L7-green fluorescent protein (L7-GFP) mouse retina (29) by using fluorescence-activated cell sorting. After FACS, 35 to 40% of the sorted cells were strongly GFP⁺, and another 30% were weakly to moderately GFP⁺; 38% were protein kinase C (PKC) (MC5)⁺ bipolar neurons; 22% were B6-30⁺ rods; 2% were HPC-1⁺ amacrine; and none were GFAP⁺ glia. Thus, this procedure enriched bipolar neurons to between 38% (by PKC expression) and 75% (by L7-promoted GFP expression).
29. M. Tomomura, D. S. Rice, J. I. Morgan, M. Yuzaki, *Eur. J. Neurosci.* **14**, 57 (2001).
30. Amacrine membranes were adsorbed onto the dish and rinsed before adding RGCs; after coculture, RGCs were trypsinized, pipetted, and centrifuged before replating, making subsequent amacrine membrane carryover unlikely. To examine membrane transfer directly, we labeled amacrine cells before membrane preparation with [³⁵S]methionine for bulk protein and with Dil for membrane lipid. RGCs cultured on these amacrine membranes and then replated per our regular protocol carried over no visible Dil, and ³⁵S was not above background. Thus, an amacrine membrane-associated signal did not simply carry over and inhibit signal axon growth but rather irreversibly signaled the embryonic neurons to decrease their intrinsic axon growth ability.
31. S. M. Rosentreter et al., *J. Neurobiol.* **37**, 541 (1998).
32. E. N. Yamasaki, A. S. Ramoa, *J. Comp. Neurol.* **329**, 277 (1993).
33. G. M. Bray, M. P. Villegas-Perez, M. Vidal-Sanz, A. J. Aguayo, *J. Exp. Biol.* **132**, 5 (1987).
34. A. J. Aguayo, M. Vidal-Sanz, M. P. Villegas-Perez, G. M. Bray, *Ann. NY Acad. Sci.* **495**, 1 (1987).
35. G. M. Bray, personal communication.
36. L. McKerracher, M. Vidal-Sanz, A. J. Aguayo, *J. Neurosci.* **10**, 641 (1990).
37. E. Y. Cho, K. F. So, *Brain Res.* **419**, 369 (1987).
38. A. M. Davies, *Nature* **337**, 553 (1989).
39. J. L. Goldberg, B. A. Barres, *Annu. Rev. Neurosci.* **23**, 579 (2000).

40. Detailed step-by-step protocols are available on request. We thank M. Cameron for gifted technical assistance, Regeneron for recombinant BDNF and CNTF, M. Lin and M. Greenberg for the adenoviral TrkB-GFP vector, M. Yuzaki for L7-GFP mice, Y. Xu and N. Davidson for the adenoviral bcl-2 vector, P. Hargrave and R. Molday for valuable antibodies, and S. Brady-Kalley for purified N-cadherin. We also thank L. Luo, J. Dugas, W. Mandemakers, K.

Christopherson, and M. Lin for thoughtful comments on the manuscript. This research was possible thanks to the support of the National Eye Institute (RO1 EY11030, B.A.B.), the March of Dimes Foundation (1-FY01-352, B.A.B.), and the NIGMS Medical Scientist Training Program (2T32GM07365; J.L.G.).

27 November 2001; accepted 4 April 2002

Trans-Synaptic Eph Receptor–Ephrin Signaling in Hippocampal Mossy Fiber LTP

Anis Contractor,^{1*} Cheryl Rogers,¹ Cornelia Maron,¹ Mark Henkemeyer,² Geoffrey T. Swanson,³ Stephen F. Heinemann¹

The site of induction of long-term potentiation (LTP) at mossy fiber–CA3 synapses in the hippocampus is unresolved, with data supporting both pre- and postsynaptic mechanisms. Here we report that mossy fiber LTP was reduced by perfusion of postsynaptic neurons with peptides and antibodies that interfere with binding of EphB receptor tyrosine kinases (EphRs) to the PDZ protein GRIP. Mossy fiber LTP was also reduced by extracellular application of soluble forms of B-ephrins, which are normally membrane-anchored presynaptic ligands for the EphB receptors. The application of soluble ligands for presynaptic ephrins increased basal excitatory transmission and occluded both tetanus and forskolin-induced synaptic potentiation. These findings suggest that PDZ interactions in the postsynaptic neuron and trans-synaptic interactions between postsynaptic EphB receptors and presynaptic B-ephrins are necessary for the induction of mossy fiber LTP.

Although it is widely agreed that expression of LTP at mossy fiber synapses occurs in the presynaptic terminal (1, 2), the site of induction of this *N*-methyl-D-aspartate (NMDA) receptor-independent form of plasticity is still not clear (3, 4). Previous data have both supported (3, 5) and excluded (4, 6, 7) a role for postsynaptic signaling pathways in the induction process. In contrast, it is generally agreed that the long-lasting alteration in synaptic strength is expressed presynaptically as an increased probability of neurotransmitter release (1, 6). If postsynaptic mechanisms do indeed underlie induction of mossy fiber LTP, retrograde signaling must exist to transduce the signal to the presynaptic nerve terminal.

The goal of our initial experiments was to determine the importance of glutamate receptor–PDZ interactions in stabilizing excitatory

transmission at hippocampal mossy fiber synapses. Intracellular perfusion of CA3 pyramidal neurons with a peptide corresponding to the carboxyl-terminal 10 amino acids of GluR2 (R2ct) to disrupt GluR2–PDZ interactions (8) had a small effect on basal synaptic transmission in some recordings, as previously described in CA1 pyramidal neurons (9, 10) (Fig. 1B). In contrast, potentiation of the excitatory postsynaptic current (EPSC) measured 25 to 30 min after tetanic stimulation was significantly smaller than in control recordings without peptide [control LTP: 220 ± 30%, *n* = 13 cells; R2ct LTP: 140 ± 11%, *n* = 18 cells, *P* < 0.01 Kolmogorov–Smirnov (K-S) test (Fig. 1)]. In control recordings, the paired-pulse ratio (PPR) of mossy fiber EPSCs, measured at a 40-ms interval between stimuli, was reduced after induction of LTP, consistent with an increase in the probability of glutamate release (6) (control PPR: 2.9 ± 0.12; LTP PPR: 2.3 ± 0.16, *n* = 12 cells, *P* < 0.01). Postsynaptic perfusion of the R2ct peptide also reduced this change in PPR (R2ct control PPR: 2.8 ± 0.14; LTP PPR: 2.5 ± 0.12, *n* = 16 cells, *P* > 0.05), in accord with the diminished potentiation after tetanic stimulation (Fig. 1). We also observed that posttetanic potentiation (PTP) immediately after tetanic stimulation was significantly smaller in recordings in

¹Molecular Neurobiology Laboratory, The Salk Institute for Biological Studies, 10010 North Torrey Pines Road, La Jolla, CA 92037, USA. ²Center for Developmental Biology and Kent Waldrep Foundation Center for Basic Neuroscience Research on Nerve Growth and Regeneration, University of Texas Southwestern Medical Center, Dallas, TX 75235, USA. ³Department of Pharmacology and Toxicology, University of Texas Medical Branch, 301 University Boulevard, Galveston, TX 77555, USA.

*To whom correspondence should be addressed. E-mail: contractor@salk.edu

REPORTS

which we perfused the R2ct peptide into the postsynaptic cell (control PTP: $840 \pm 70\%$; R2ct PTP: $510 \pm 67\%$, $P < 0.01$). There was no difference in the suppression of mossy fiber EPSCs by the group II mGluR agonist LCCG-1 ($P > 0.05$), which ruled out the possibility that the observed effects were due to significant contamination by non-mossy fiber inputs.

To test the specificity of the R2ct peptide effect, we made recordings during intracellular perfusion of a scrambled peptide without a PDZ recognition consensus sequence (R2ctSC). Basal EPSC amplitudes were stable in these experiments, LTP was elicited by tetanic stimulation [$200 \pm 11\%$, $n = 10$ cells, $P > 0.05$ (K-S test)] (Fig. 1D), and PPR was reduced after induction of LTP (control PPR: 3.1 ± 0.19 ; LTP PPR: 2.4 ± 0.10 , $n = 10$ cells, $P < 0.01$). To investigate the type of PDZ protein that was involved in mediating mossy fiber LTP, we made recordings while perfusing CA3 neurons with a phosphorylated GluR2/3 peptide (R2ctPO₄), which competes for binding to PICK1, but not GRIP (11, 12). Tetanic stimulation produced normal potentiation of EPSCs after perfusion of R2ctPO₄ [$210 \pm 19\%$, $n = 10$ cells, $P > 0.05$ (K-S test)] as compared to control LTP (Fig. 1D) and a reduction in PPR (control PPR: 3.0 ± 0.18 ; LTP PPR: 2.5 ± 0.16 , $n = 10$, $P < 0.05$).

Because our results suggested that GRIP interactions in the postsynaptic neuron affected presynaptic function after induction of LTP, we examined potential retrograde signaling systems whose component molecules contain PDZ-binding motifs. One such pair of candidate molecules was the Eph receptor tyrosine kinases (EphRs) and their intercellular binding partners, the ephrin ligands (13). These molecules are expressed at synapses in the CA3 region of the hippocampus (14) and interact with the same PDZ proteins as α -amino-3-hydroxy-5-methyl-4-isoxazolepropionate (AMPA) receptors, albeit at different PDZ domains (15).

We perfused CA3 pyramidal neurons with peptides corresponding to the PDZ-binding carboxyl terminals of one of the representative members of the two families of EphRs, EphA7 or EphB2. Introduction of EphA7 peptide did not affect either short-term plasticity or LTP [control PPR: 2.8 ± 0.14 ; LTP PPR: 2.3 ± 0.17 , $P < 0.05$; PTP: $820 \pm 130\%$; LTP: $230 \pm 32\%$, $n = 8$ cells, $P > 0.05$ (K-S test)] (Fig. 2, A through D). In contrast, perfusion with the EphB2 peptide significantly depressed both PTP ($450 \pm 69\%$, $n = 10$ cells, $P < 0.05$) and tetanus-induced LTP [$124 \pm 12\%$, $n = 10$ cells, $P < 0.01$ (K-S test)]. The PPR after tetanic stimulation was identical to that at the end of the basal recording period (control PPR: 2.5 ± 0.17 ; LTP PPR: 2.5 ± 0.19 , $n = 10$ cells, $P > 0.05$).

We examined the possibility that the R2ct peptide directly disrupted binding of Eph receptors to PDZ domain 6 of GRIP (15) rather than interacting specifically with the GluR2 subunit-binding PDZ 4 and 5 domains (16). We performed in vitro competitive binding experiments between GRIP PDZ domain

fragments and the EphB2 carboxyl-terminal fusion protein (8) using the peptides from our physiological studies. [³⁵S]EphB2 binding to GRIP (PDZ 4 through 6) was effectively displaced by the R2ct peptide with an inhibition constant (K_i) of 106 nM (obtained from fitting the data points with the Hill equation)

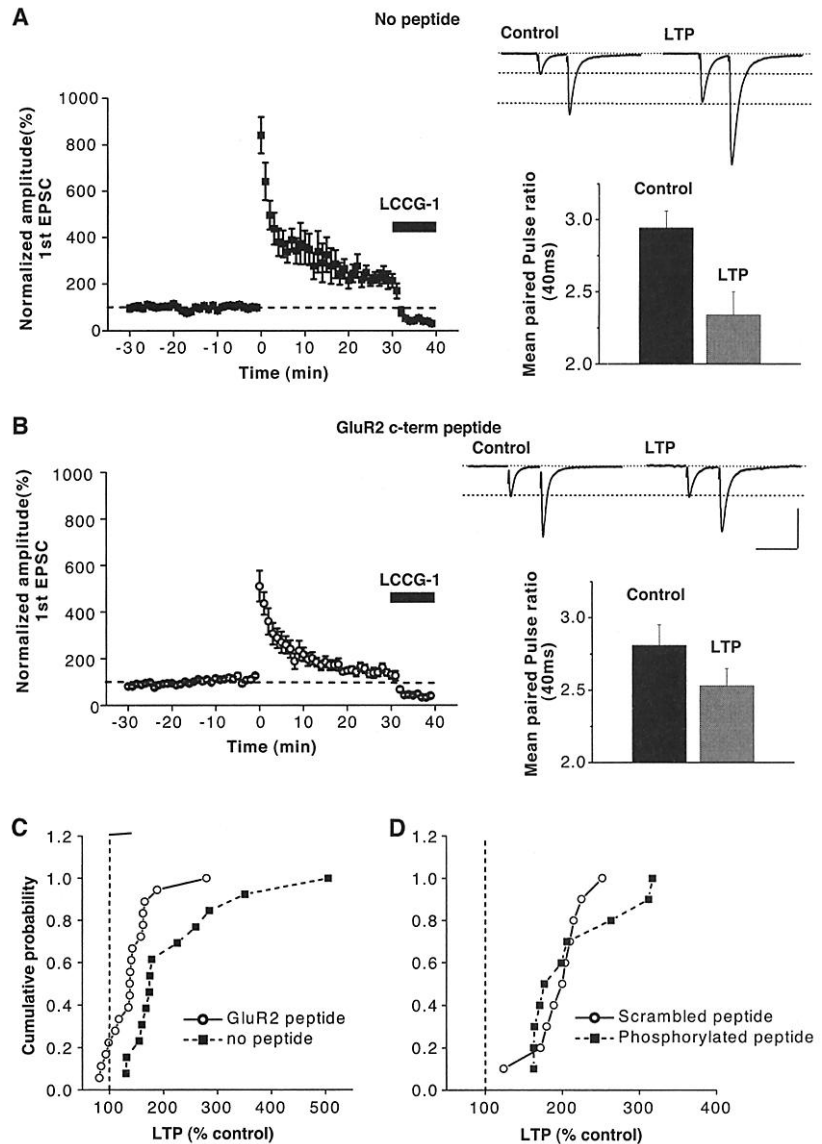


Fig. 1. GluR2 carboxyl-terminal peptide occluded mossy fiber LTP in the hippocampus. **(A)** (left panel) Time course of mossy fiber LTP from 13 experiments with no peptide (protease inhibitors only) included in the patch electrode. Significant potentiation of the first EPSC was observed 20 to 30 min after tetanus. Application of the group II mGluR agonist LCCG-1 at the end of each experiment inhibited the EPSC, signifying EPSCs of mossy fiber origin (34). Sample EPSC traces from one recording during the control period (–30 to 0 min) and after LTP induction (20 to 30 min) are shown in the upper right panel. Mean PPRs of EPSCs were measured at an interval of 40 ms (lower right panel). **(B)** Time course of mossy fiber LTP from 18 experiments in which the GluR2 carboxyl-terminal peptide (R2ct) was included in the patch electrode. Little potentiation was observed between 25 and 30 min after tetanus. Sample traces from one recording are shown (top right panel). Calibration [for (A) and (B)]: x axis, 50 ms; y axis, 500 pA. PPRs were not significantly different after induction of LTP, $P > 0.05$ (bottom right panel). **(C)** Cumulative probability histogram of mossy fiber LTP measured as percent increase from control 25 to 30 min after tetanic stimulation. Recordings in which the R2ct peptide was included (open circles) showed significantly less potentiation than recordings without peptide introduced into the postsynaptic cell (solid squares) ($P < 0.01$). **(D)** Cumulative probability histogram for mossy fiber recordings in which the scrambled peptide (R2ctSC) and the phosphorylated peptide (R2ctPO₄) were introduced into the postsynaptic neuron.

REPORTS

(Fig. 2E, top panel). The EphB2 peptide was more potent (K_i value of 43 nM, Fig. 2E, top panel). The peptides that did not occlude LTP, R2ctSC and R2ctPO₄, did not inhibit binding of EphB2 to GRIP in this assay at concentrations as high as 10 μ M (Fig. 2E, top

panel). To test whether the R2ct peptide displaced EphB2 binding directly from PDZ 6, rather than through an indirect allosteric modulation, we repeated these experiments with a GRIP fragment containing PDZ 6 alone. The GluR2 peptide displaced EphB2

binding to this fragment, with a K_i value of 155 nM (Fig. 2E, bottom panel). Our findings correspond to a previous report indicating that a short 13-amino acid fragment of GluR2 bound to PDZ 6 of the AMPA binding protein (ABP), a splice variant of GRIP (17).

In order to ascertain whether EphR and GluR2 can be bound to the same complex in brain, we performed a glutathione *S*-transferase (GST) pull-down assay by incubating the EphB2 carboxyl terminal with rat brain membranes (8). GluR2 specifically associated with EphB2 but not with GST alone or with NMDA receptors (Fig. 2F), suggesting that EphB2 and GluR2 can potentially bind to the same GRIP complex in vivo. We also found that the GluR2 carboxyl terminal (50 amino acids), unlike the 10-amino acid R2ct peptide, did not interact with PDZ domain 6 of GRIP in yeast-two hybrid assays (18) as previously described (16).

The EphB2 peptide might interfere with binding of other proteins to GRIP PDZ domain 6. To determine more directly whether EphB receptors play a role in LTP, we included an antibody directed against the carboxyl terminal of EphB2 (EphB2a/b) in our intracellular recording solution (Fig. 3A). Plasticity after perfusion with the EphB2 antibody was compared to two control conditions in which CA3 pyramidal neurons were either perfused with EphB2 antibody preabsorbed with a GST fusion protein of the carboxyl-terminal domain of EphB2 (pre-EphB2a/b) or with an antibody directed against the amino terminus of the EphB1 receptor (EphB1a/b), which is located extracellularly. Inclusion of EphB2a/b had no effect on basal transmission during a 30-min baseline recording period. However, LTP measured at 20 to 30 min after tetanus was significantly impaired as compared to interleaved control experiments with the pre-EphB2a/b or EphB1a/b [EphB2a/b LTP: $130 \pm 14\%$, $n = 12$ cells; pre-EphB2a/b LTP: $210 \pm 17\%$, $n = 8$ cells, $P < 0.05$; EphB1a/b LTP: $210 \pm 15\%$, $n = 11$ cells, $P < 0.05$ (K-S test)] (Fig. 3, A through E). Similar to previous results, PPRs decreased after LTP in the control antibody recordings but did not change significantly when LTP was impaired with the EphB2a/b (EphB2a/b control PPR: 2.8 ± 0.2 ; EphB2a/b LTP PPR: 2.9 ± 0.2 , $n = 12$ cells, $P > 0.05$) (Fig. 3F).

Our initial results in which the R2ct peptide occluded LTP might reflect participation of AMPA receptor-PDZ interactions in the induction of mossy fiber LTP. We therefore perfused neurons with antibody directed against the carboxyl-terminal domain of the GluR2 and GluR3 receptor subunits (GluR2a/b). Mossy fiber LTP was normal when this antibody was included in the patch electrode [$210 \pm 17\%$, $n = 10$ cells, $P > 0.05$ (K-S test)] (Fig. 3, C through F). We also observed

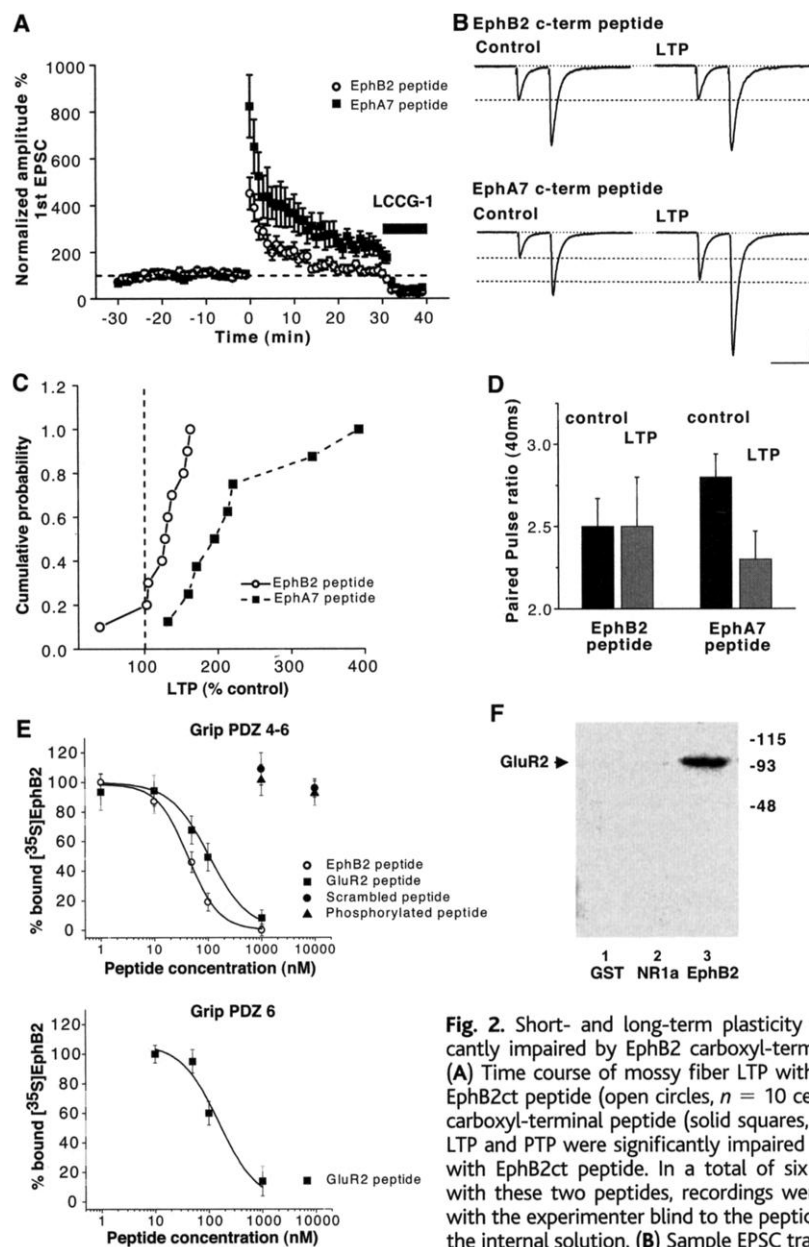


Fig. 2. Short- and long-term plasticity were significantly impaired by EphB2 carboxyl-terminal peptide. (A) Time course of mossy fiber LTP with inclusion of EphB2ct peptide (open circles, $n = 10$ cells) or EphA7 carboxyl-terminal peptide (solid squares, $n = 8$ cells). LTP and PTP were significantly impaired in recordings with EphB2ct peptide. In a total of six experiments with these two peptides, recordings were performed with the experimenter blind to the peptide included in the internal solution. (B) Sample EPSC traces from one recording before and after induction of LTP with EphB2ct peptide (top) or EphA7 peptide (bottom). Calibration: x axis, 50 ms; y axis, 100 pA (EphB2), 200 pA (EphA7). (C) Cumulative probability histogram of percent change in EPSC 20 to 30 min after induction of LTP with EphB2 (open circles) and EphA7 (solid squares) peptides. (D) PPR after LTP induction was significantly reduced in recordings with EphA7 peptide but not in recordings with EphB2ct peptide. (E) (Top) Binding of labeled [³⁵S]EphB2 c-term to GRIP(PDZ4–6) competed with increasing concentrations of peptide. Each data point represents the normalized mean of four experiments. Data points for the EphB2ct peptide (open circles) and the R2ct peptide (solid squares) are fitted to the Hill equation. The EphB2ct peptide inhibited binding with a K_i of 43 nM, and the R2ct peptide inhibited binding with a K_i of 106 nM. Labeled EphB2 was not displaced from GRIP(PDZ4–6) by scrambled (solid circles) or phosphorylated peptides (solid triangles) at concentrations up to 10 μ M peptide. (Bottom) Displacement of [³⁵S]EphB2 from GRIP (PDZ 6 only) by the R2ct peptide ($K_i = 155$ nM). (F) Pull-down experiments in rat brain membranes using fusion proteins containing GST (lane 1), the NR1a carboxyl terminal (lane 2), or the GST EphB2 carboxyl terminal (lane 3) revealed that GluR2 specifically associated with EphB2.

REPORTS

a concomitant decrease in PPR after LTP induction (control PPR: 3.1 ± 0.2 ; LTP PPR: 2.4 ± 0.2 , $n = 10$ cells, $P < 0.05$).

EphB receptors transduce signals bidirectionally by interacting with membrane-anchored ephrin B ligands expressed on adjacent cells. We tested whether trans-synaptic Eph-ephrin signaling underlies plasticity at the mossy fiber synapse, using soluble chimeric protein reagents containing the extracellular domains of EphB2 receptors (EphB2-Fc), ephrin B1 ligands (ephrin B1-Fc), or EphA5 receptors (EphA5-Fc) fused to the Fc region of human immunoglobulin G (IgG) (19–22). Although application of preclustered Eph-Fc and ephrin-Fc reagents can strongly activate reverse or forward signaling, respectively, the dimeric forms used in our study act primarily as blocking reagents to prevent signaling and display only weak agonist activity (23). Extracellular bath application of the EphB2-Fc fusion protein ($5 \mu\text{g/ml}$), which binds to presynaptic ephrins, for a 20-min period during baseline recording resulted in a $145 \pm 13\%$ increase in the basal EPSC amplitude (Fig. 4A). In addition, there was a small nonsignificant reduction in the baseline PPR. Potentiation of EPSCs after subsequent tetanic stimulation was significantly reduced to a magnitude similar to that observed in the peptide experiments (EphB2-Fc LTP: $134 \pm 13\%$, $n = 7$ cells, $P < 0.05$), and the PPR was not reduced from baseline values (control PPR: 2.5 ± 0.3 ; LTP PPR: 2.2 ± 0.2 , $n = 7$ cells, $P > 0.05$) (Fig. 4, B and C). In a separate set of experiments, the EphB2-Fc-mediated potentiation of mossy fiber EPSCs was not observed after prior tetanic stimulation (Fig. 4A).

Bath application of the ephrin B1-Fc chimera ($5 \mu\text{g/ml}$), which binds postsynaptic Eph receptors, did not alter the baseline EPSC amplitudes (Fig. 4D). However, LTP after tetanus again was reduced in the presence of ephrin B1-Fc [$139 \pm 12\%$, $n = 6$ cells, $P < 0.05$ (K-S test) as compared to control LTP] (Fig. 4D). In the presence of both Fc fusion proteins, PTP was significantly impaired (EphB2-Fc PTP: $420 \pm 85\%$; ephrin B1-Fc PTP: $430 \pm 100\%$). In contrast, baseline EPSC amplitudes and short- and long-term plasticity were not affected by bath application of the EphA5-Fc (EphA5 LTP: 221 ± 32 , $n = 6$ cells, $P > 0.05$; as compared to control LTP) (Fig. 4F). In summary, these data indicate that dimeric EphB-Fc fusion proteins can directly activate presynaptic ephrin B ligands and potentiate mossy fiber synaptic transmission, thus occluding subsequent tetanus-induced LTP. Soluble ephrin-Fc ligands appear to block tetanus-induced retrograde signaling from postsynaptic EphB receptors to presynaptic ephrin ligands and thereby impair mossy fiber plasticity.

Activation of protein kinase A (PKA) by

application of forskolin enhances mossy fiber synaptic transmission and occludes further tetanus-induced LTP (24, 25). There is strong evidence that this enzyme's actions are in the presynaptic terminal; however, a postsynaptic role for PKA has been described (3). We tested whether forskolin-mediated potentiation was affected by disruption of Eph/ephrin signaling at mossy fiber synapses. Forskolin potentiated mossy fiber EPSCs 20 to 30 min

after forskolin application by $275 \pm 38\%$, $n = 5$ cells (Fig. 4, G and I). Blockade of the interaction between postsynaptic Eph receptors and presynaptic ephrins by preapplication of ephrin B1-Fc protein did not result in a significant block of potentiation ($219 \pm 15\%$, $n = 5$ cells, $P > 0.05$) (Fig. 4, H and I), suggesting that PKA acts downstream of Eph receptor binding to ephrins. When we applied ligands for the presynaptic ephrins (EphB2-

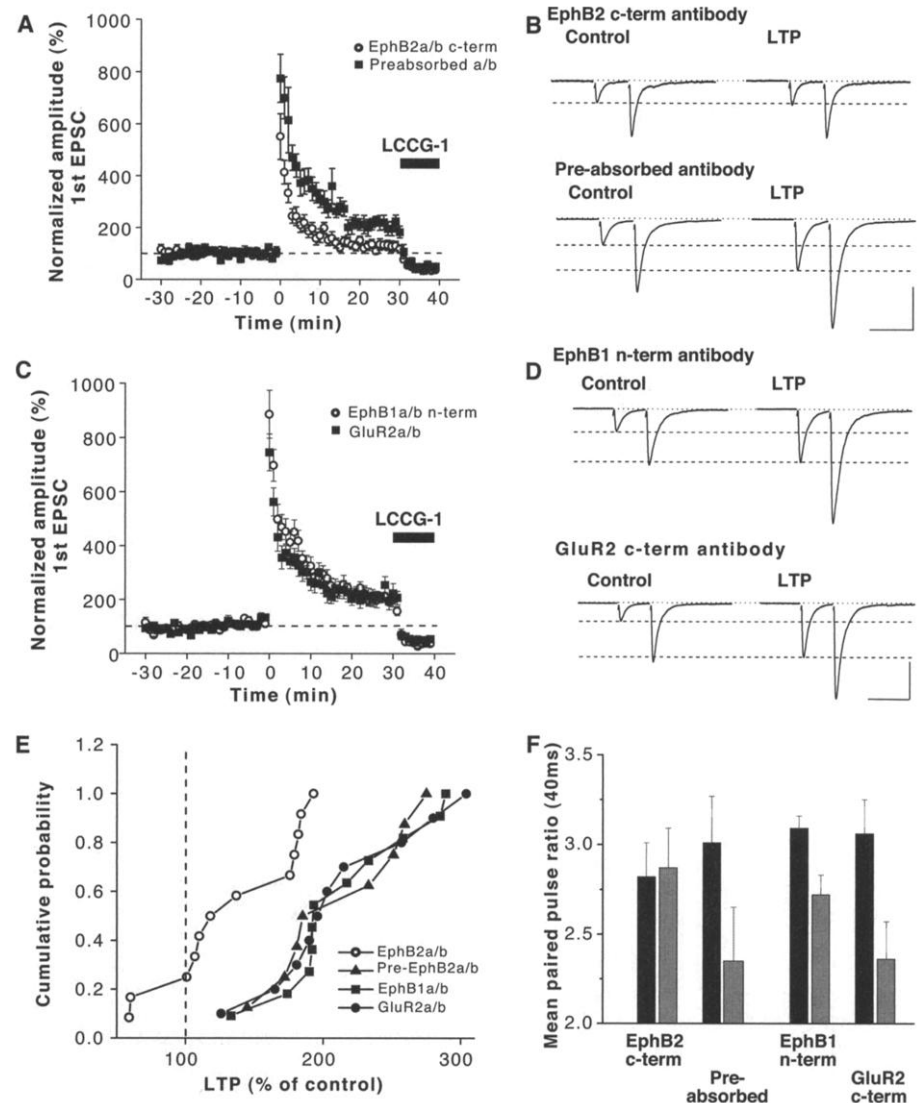


Fig. 3. Mossy fiber LTP was occluded by inclusion of an antibody against the carboxyl terminal of the EphB2 receptor. (A) Time course of mossy fiber LTP when either EphB2 c-term antibody ($20 \mu\text{g/ml}$) (open circles, 12 recordings) or preabsorbed EphB2 antibody (filled squares, 8 recordings) were included in the patch electrode. A significant potentiation of the EPSC was observed at 20–30 min with the preabsorbed antibody, whereas LTP was impaired when EphB2 c-term antibody was included in the patch electrode. (B) Sample traces before and after LTP induction from individual recordings with EphB2 antibody (top) or preabsorbed antibody (bottom). Calibration: x axis, 50 ms; y axis, 400 pA (EphB2 antibody), 600 pA (preabsorbed antibody). (C) Time course of LTP in recordings in which EphB1 amino terminal antibody (open circles) or GluR2/3 carboxyl-terminal antibody (solid squares) was included in the patch electrode. (D) Sample traces from recordings with EphB1 antibody (top) and GluR2/3 antibody (bottom). Calibration: x axis, 50 ms; y axis, 375 pA (EphB1 antibody), 500 pA (GluR2/3 antibody). (E) Cumulative probability histogram of LTP with inclusion of antibodies. (F) PPRs were significantly reduced after LTP in each case, except when EphB2 c-term antibody was present in the patch electrode. PPR values for each antibody were EphB2a/b: control 2.8 ± 1.9 , LTP 2.9 ± 0.2 ; pre-EphB2a/b: control 3.1 ± 0.2 , LTP 2.4 ± 0.2 ; EphB1a/b: control 3.1 ± 0.1 , LTP 2.7 ± 0.1 ; GluR2/3a/b: control 3.1 ± 0.2 , LTP 2.4 ± 0.2 .

REPORTS

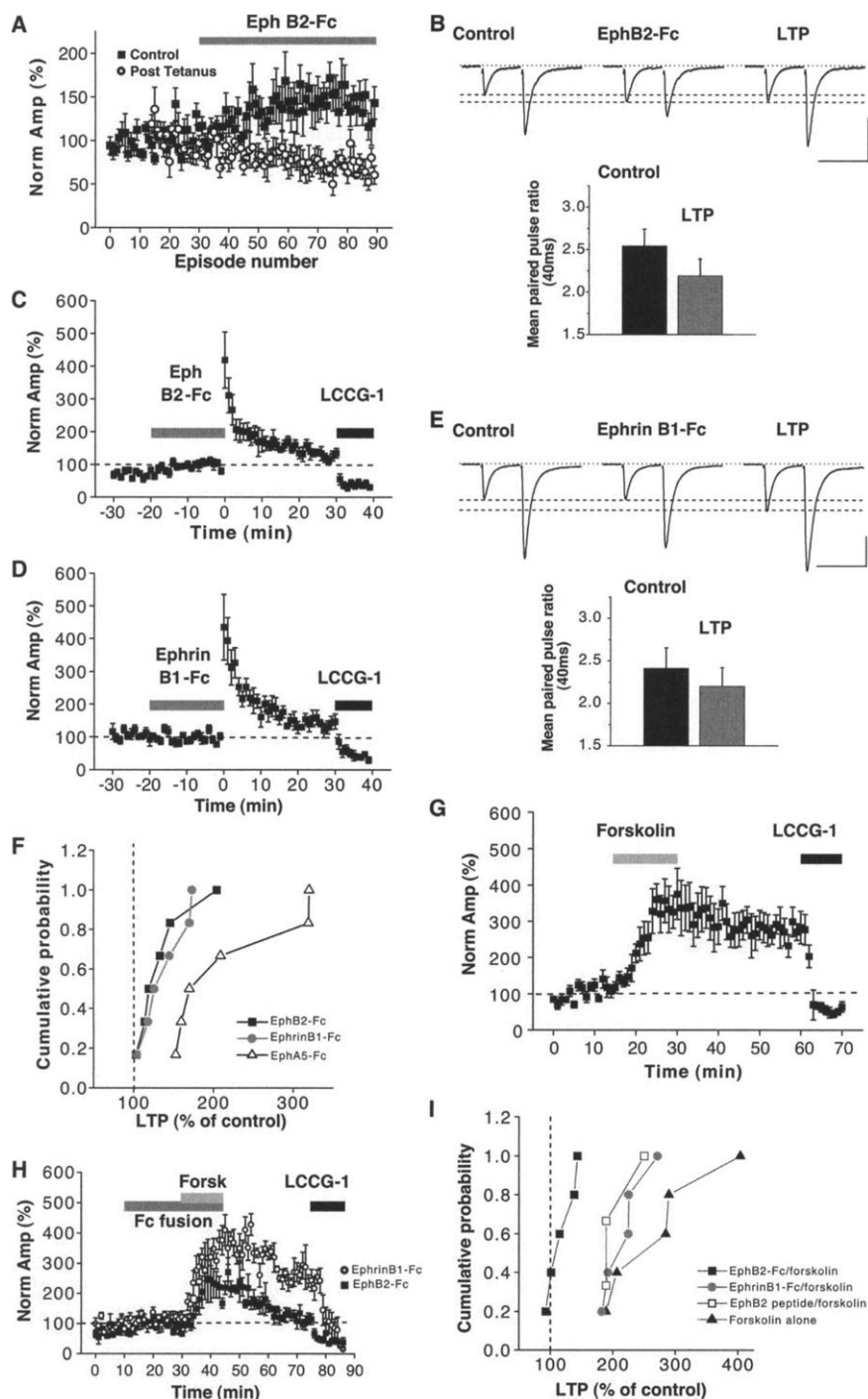


Fig. 4. Application of soluble Fc fusion proteins of Eph receptors and ephrins occluded mossy fiber LTP. **(A)** Extracellular application of EphB2-Fc significantly increased basal synaptic transmission during the pretetanic control recordings (solid squares). EphB2-Fc-mediated potentiation of transmission was not observed if the chimeric fusion protein was applied after LTP induction (open circles) ($n = 5$ cells). **(B)** Sample traces before and during application of EphB2-Fc and after LTP induction (top). PPRs were not significantly reduced after LTP induction (bottom). **(C)** Prior application of EphB2-Fc occluded subsequent tetanus-induced LTP. **(D)** Application of ephrin B1-Fc did not affect basal transmission but LTP induction was significantly impaired. **(E)** Sample traces before LTP, during application of ephrin B1-Fc, and after LTP induction. PPRs measured at 40-ms interstimulus intervals were not significantly changed after LTP. **(F)** Cumulative probability histogram of LTP induced during application of EphB2-Fc, ephrin B1-Fc and EphA5-Fc. Significant potentiation was seen in recordings in the presence of EphA5-Fc along with a significant decrease in PPR (EphA5-Fc control: 2.5 ± 0.2 ; EphA5-Fc LTP: 1.9 ± 0.1 , $n = 6$ cells, $P < 0.05$). **(G)** Forskolin-mediated enhancement of mossy fiber transmission. **(H)** Application of ephrin B1-Fc before forskolin did not affect PKA-dependent potentiation; however, prior application of EphB2-Fc occluded subsequent forskolin effects. **(I)** Cumulative probability for forskolin enhancement of mossy fiber transmission with prior application of Fc fusion proteins or inclusion of EphB2 peptide in the recording electrode.

Fc), we again saw a significant potentiation of baseline amplitudes ($148 \pm 19\%$, $n = 5$ cells). In these experiments, subsequent application of forskolin caused a transient potentiation of mossy fiber EPSCs; however, this decayed back to baseline levels 30 min after washout ($118 \pm 10\%$, $n = 5$ cells, $P < 0.01$; as compared to control forskolin) (Fig. 4, H and I). These data demonstrate that activation of presynaptic ephrins occludes further PKA-mediated potentiation of mossy fiber transmission, suggesting that ephrins and PKA are part of the same presynaptic signaling pathway that leads to mossy fiber potentiation. This hypothesis was further supported by recordings with the EphB2 peptide in the recording electrode. Unlike tetanus-induced LTP, which was blocked by this peptide, forskolin-mediated potentiation was normal ($209 \pm 20\%$, $n = 3$ cells, $P > 0.05$) (Fig. 4I).

As EphRs and ephrins interact promiscuously within their own subfamilies (26), our experiments did not allow us to identify a particular member of the EphB family as critically relevant to mossy fiber LTP. We attempted to determine whether EphB2 receptors play an important role by carrying out recordings from gene-targeted mice lacking EphB2 protein and mice expressing a truncated form of EphB2 that lacked the carboxyl-terminal PDZ binding motif (27). EphB2 null mutants, at the ages used in our recordings, had a diffuse CA3 pyramidal cell layer, with many pyramidal neurons located ectopically in the stratum radiatum. In recordings from neurons in the pyramidal cell layer, we could find mossy fiber inputs in only a subset of cells. Because of these clear developmental abnormalities, these studies on null mutant mice did not shed light on the possible role of EphB2 receptors in mossy fiber LTP. We also made recordings from EphB2 carboxyl-terminal truncation mutants. There were no obvious gross anatomical abnormalities in the CA3 region of these mice, and mossy fiber inputs were easily identifiable. Mossy fiber LTP in these mice was normal as compared to recordings from heterozygous or wild-type littermates [EphB2^{cterm}-/- LTP: $230 \pm 24\%$, $n = 5$ cells; wild-type/heterozygote LTP: $200 \pm 28\%$, $n = 7$ cells, $P > 0.05$ (K-S test)]. Other members of the EphB receptor family are expressed in the CA3 and are likely to compensate for the mutation in these mice.

Recently, EphB receptors have been demonstrated to interact directly with NMDA receptors (28). Recordings from EphB2^{-/-} receptor mice have revealed deficits in several forms of NMDA receptor plasticity (29, 30) due to a decrease in NMDA receptor expression at synapses (29). Eph receptors also directly modulate NMDA receptor function by inducing tyrosine phosphorylation of NMDA receptors. This may directly modify NMDA receptor calcium influx and NMDA-dependent synaptic plasticity (31).

Our data now provide evidence for a function for Eph receptors and ephrins that establishes roles in NMDA-independent forms of synaptic plasticity.

Our results provide strong support for postsynaptic induction of mossy fiber LTP and are consistent with earlier reports in which tetanic stimulation elicited postsynaptic rises in calcium, triggering induction of LTP (3, 5). Furthermore, we have identified a retrograde signaling pathway, EphB receptor–ephrin B ligand interaction, that links postsynaptic induction with presynaptic expression of long-term changes in release probability. These results suggest a model for induction of mossy fiber LTP initiated by activation of kainate and/or metabotropic glutamate receptors upon tetanic stimulation of mossy fibers (3, 32, 33) and subsequent postsynaptic intracellular signaling, resulting in the promotion of clustering of EphB receptors by GRIP or a similar molecule. This interaction allows EphRs to associate with and activate reverse signaling by presynaptic ephrin-B ligands, which may then regulate downstream events, including those mediated

by PKA, and ultimately results in an increase in glutamate release in mossy fiber terminals.

References and Notes

1. M. G. Weisskopf, R. A. Nicoll, *Nature* **376**, 256 (1995).
2. Z. Xiang, A. C. Greenwood, E. W. Kairiss, T. H. Brown, *J. Neurophysiol.* **71**, 2552 (1994).
3. M. F. Yeckel, A. Kapur, D. Johnston, *Nature Neurosci.* **2**, 625 (1999).
4. J. Mellor, R. A. Nicoll, *Nature Neurosci.* **4**, 125 (2001).
5. S. Williams, D. Johnston, *Neuron* **3**, 583 (1989).
6. R. A. Zalutsky, R. A. Nicoll, *Science* **248**, 1619 (1990).
7. H. Katsuki, S. Kaneko, A. Tajima, M. Satoh, *Neurosci. Res.* **12**, 393 (1991).
8. Materials and methods are available as supporting material on Science Online.
9. M. I. Daw *et al.*, *Neuron* **28**, 873 (2000).
10. C. H. Kim, H. J. Chung, H. K. Lee, R. L. Huganir, *Proc. Natl. Acad. Sci. U.S.A.* **98**, 11725 (2001).
11. S. Matsuda, S. Mikawa, H. Hirai, *J. Neurochem.* **73**, 1765 (1999).
12. H. J. Chung, J. Xia, R. H. Scannevin, X. Zhang, R. L. Huganir, *J. Neurosci.* **20**, 7258 (2000).
13. R. Klein, *Curr. Opin. Cell Biol.* **13**, 196 (2001).
14. M. T. Moreno-Flores, F. Wandosell, *Neuroscience* **91**, 193 (1999).
15. R. Torres *et al.*, *Neuron* **21**, 1453 (1998).
16. H. Dong *et al.*, *Nature* **386**, 279 (1997).
17. S. Srivastava *et al.*, *Neuron* **21**, 581 (1998).
18. A. Contractor *et al.*, data not shown.
19. S. J. Holland *et al.*, *Nature* **383**, 722 (1996).
20. K. Bruckner, E. B. Pasquale, R. Klein, *Science* **275**, 1640 (1997).

21. Q. Lu, E. E. Sun, R. S. Klein, J. G. Flanagan, *Cell* **105**, 69 (2001).
22. C. A. Cowan, M. Henkemeyer, *Nature* **413**, 174 (2001).
23. E. Stein *et al.*, *Genes Dev.* **12**, 667 (1998).
24. Y. Y. Huang, X. C. Li, E. R. Kandel, *Cell* **79**, 69 (1994).
25. M. G. Weisskopf, P. E. Castillo, R. A. Zalutsky, R. A. Nicoll, *Science* **265**, 1878 (1994).
26. N. W. Gale *et al.*, *Neuron* **17**, 9 (1996).
27. M. Henkemeyer *et al.*, *Cell* **86**, 35 (1996).
28. M. B. Dalva *et al.*, *Cell* **103**, 945 (2000).
29. J. T. Henderson *et al.*, *Neuron* **32**, 1041 (2001).
30. I. C. Grunwald *et al.*, *Neuron* **32**, 1027 (2001).
31. M. A. Takasu, M. B. Dalva, R. E. Zigmond, M. E. Greenberg, *Science* **295**, 491 (2002).
32. Z. A. Bortolotto *et al.*, *Nature* **402**, 297 (1999).
33. A. Contractor, G. Swanson, S. F. Heinemann, *Neuron* **29**, 209 (2001).
34. H. Kamiya, H. Shinozaki, C. Yamamoto, *J. Physiol.* **493**, 447 (1996).
35. This work was supported by grants from the NIH National Institute of Mental Health (A.C., M.H.), National Alliance for Research on Schizophrenia and Depression (C.R., G.T.S.) and NIH National Institute of Neurological Disorders and Stroke (S.F.H.). We thank W. Che for technical assistance and R. Allen for generating His-GRIP protein.

Supporting Online Material

www.sciencemag.org/cgi/content/full/296/5574/1864/DC1
Materials and Methods

17 December 2001; accepted 26 April 2002

Two-Photon Imaging of Lymphocyte Motility and Antigen Response in Intact Lymph Node

Mark J. Miller,¹ Sindy H. Wei,¹ Ian Parker,^{2*} Michael D. Cahalan^{1*†}

Lymphocyte motility is vital for trafficking within lymphoid organs and for initiating contact with antigen-presenting cells. Visualization of these processes has previously been limited to *in vitro* systems. We describe the use of two-photon laser microscopy to image the dynamic behavior of individual living lymphocytes deep within intact lymph nodes. In their native environment, T cells achieved peak velocities of more than 25 micrometers per minute, displaying a motility coefficient that is five to six times that of B cells. Antigenic challenge changed T cell trajectories from random walks to “swarms” and stable clusters. Real-time two-photon imaging reveals lymphocyte behaviors that are fundamental to the initiation of the immune response.

The process by which lymphocytes transit through organized lymphoid tissues is crucial to the immune response, but it has not been amenable to direct experimental investigation and remains poorly understood (1). During transit, T lymphocytes can encounter antigen-presenting cells (APCs), take up residence in specific regions of lymphoid tissue, or reenter the circulation. *In vivo* studies at a macro-

scopic level with cannulated lymphatic vessels have provided population measurements of lymphocyte recirculation under physiological conditions (1). At the cellular and molecular level, our understanding of the immune response has been greatly enhanced by studies of cultured lymphocytes in artificial two- and three-dimensional (3D) systems (2, 3). *In vitro* systems, however, cannot replicate local environmental factors within intact lymphoid organs that shape the antigen recognition process, the transit of lymphocytes through the tissue, and the development of subsequent effector functions (4). To bridge this gap between *in vivo* and *in vitro* approaches, we used two-photon microscopy

(5, 6) to image individual living T and B lymphocytes deep within the intact lymph node.

Purified T and B cells from donor BALB/c mice were labeled with green [5- (and 6-) carboxyfluorescein diacetate succinyl ester (CFSE)] or red (5-(and-6)-(((4-chloromethyl) benzoyl)amino)tetramethylrhodamine) (CMTMR)] fluorescent dyes and injected into the tail vein of recipient mice (7). Subsequent two-photon imaging (8) of isolated, superfused lymph nodes showed the expected localization of B cells within primary follicles and of T cells predominantly in the interfollicular spaces of the diffuse cortex (Fig. 1, A and B). Individual cells could be resolved and tracked to depths of up to 350 μm beneath the capsular surface (Fig. 1, C and D), and their differing morphologies were readily distinguished (Fig. 1, E and F). In other experiments, lymph nodes were prestained with CMTMR to visualize the distribution of CFSE-stained T cells with respect to the reticular fiber network (Fig. 1G) (3D rotation is shown in Movie S1).

Dynamic changes in the locomotion of T and B cells were tracked with time-lapse 3D imaging. At room temperature, lymphocytes were nonmotile and spherical, but on warming they adopted polarized shapes and moved with velocities that were steeply dependent on temperature and were maximal near the physiological body temperature (Movie S2). Most T cells progressed by a series of repeated lunges, becoming elongated while moving rapidly and balling up when paused (Fig. 2, A and C; Movie S3). In contrast, B cells followed mean-

¹Department of Physiology and Biophysics, ²Department of Neurobiology and Behavior, University of California, Irvine, CA 92697–4561, USA.

*These authors contributed equally to this work.

†To whom correspondence should be addressed. E-mail: mcahalan@uci.edu